

A Giant Bulk-Type Dresselhaus Splitting with 3D Chiral Spin Texture in IrBiSe

Zhonghao Liu,* Setti Thirupathiah, Alexander N. Yaresko, Satya Kushwaha, Quinn Gibson, Wei Xia, Yanfeng Guo, Dawei Shen, Robert J. Cava,* and Sergey V. Borisenko*

Materials with giant spin splitting are desired for spintronic applications. The fabrications of spintronic devices from half metals with one spin direction are often hampered, however, by stray magnetic fields, domain walls, short spin coherence times, scattering on magnetic atoms or magnetically active interfaces, and other characteristics that come along with the magnetism. The surfaces of topological insulators, or Dirac/Weyl semimetals, could be an alternative, but production of high-quality thin films without the presence of the bulk states at the Fermi energy remains very challenging. Here, by utilizing angle-resolved photoemission spectroscopy, a record-high Dresselhaus spin–orbit splitting of the bulk state in the nonmagnetic IrBiSe is found. The band structure calculations indicate that the splitting band is fully spin-polarized with 3D chiral spin texture. As a source of spin-polarized electrons, lightly doped IrBiSe is expected to generate electric-field-controlled spin-polarized currents, free from back scattering, and could host triplet and Fulde–Ferrel–Larkin–Ovchinnikov (FFLO) superconductivity.

semiconductors,^[21–27] metals,^[28–30] and alloys.^[31] The former are magnetic, and the spins are usually oriented along a single global axis, thus limiting possible applications. The latter have more flexible spin textures, but are essentially 2D with crystal surfaces highly sensitive to the environment, often tending to degrade rapidly over time. Recently, several compounds have been reported that show giant spin splitting of the bulk bands; however, such materials either suffer from the possibility of surface–bulk scattering, as their band structures include both bulk and surface states in the vicinity of the Fermi energy (E_F), or very small momentum separation of the states with different spin orientations.^[25–27,31–35] Thus, novel materials without these drawbacks would be advantageous for addressing fundamental questions of physics and modern spintronics.


Materials where electrons have different energies and momenta depending on their spin orientations have significant application potential in spintronic devices.^[1–21] Manipulation of the spin degrees of freedom is best when such spin polarization and spin splitting of the electron energy bands is very strong. This strong spin differentiation is usually detected in half metals^[7–13] and on the surfaces of topological insulators or semimetals,^[14–20]

Herein, we present nonmagnetic IrBiSe with a unique electronic structure, featuring a giant (≈ 0.3 eV) Dresselhaus^[36] spin–orbit splitting of the bulk bands near E_F with an enormous momentum offset of 0.44 \AA^{-1} and peculiar 3D chiral spin texture.

The crystal structure of IrBiSe belongs to a noncentrosymmetric simple cubic space group [$P213$ (No. 198)], which is a derivative of the structure of fool's gold, FeS_2 (i.e., it is

Prof. Z. Liu, Prof. S. Thirupathiah, Prof. S. V. Borisenko
 Institute for Solid State Research
 IFW Dresden
 D-01171 Dresden, Germany
 E-mail: lzh17@mail.sim.ac.cn; s.borisenko@ifw-dresden.de

Prof. Z. Liu, Prof. D. Shen
 State Key Laboratory of Functional Materials for Informatics and Center for Excellence in Superconducting Electronics
 SIMIT
 Chinese Academy of Sciences
 Shanghai 200050, China

 The ORCID identification number(s) for the author(s) of this article can be found under <https://doi.org/10.1002/pssr.201900684>.

© 2020 The Authors. Published by WILEY-VCH Verlag GmbH & Co. KGaA, Weinheim. This is an open access article under the terms of the Creative Commons Attribution License, which permits use, distribution and reproduction in any medium, provided the original work is properly cited.

DOI: 10.1002/pssr.201900684

Prof. S. Thirupathiah
 Solid State and Structural Chemistry Unit
 Indian Institute of Science, Bangalore
 Karnataka 560012, India

Prof. A. N. Yaresko
 Department of Quantum Materials
 Max-Planck-Institute for Solid State Research
 Heisenbergstrasse 1, Stuttgart 70569, Germany

Prof. S. Kushwaha, Prof. Q. Gibson, Prof. R. J. Cava
 Department of Chemistry
 Princeton University
 Princeton, NJ 08544, USA
 E-mail: rcava@princeton.edu

Dr. W. Xia, Prof. Y. Guo
 School of Physical Science and Technology
 ShanghaiTech University
 Shanghai 200031, China

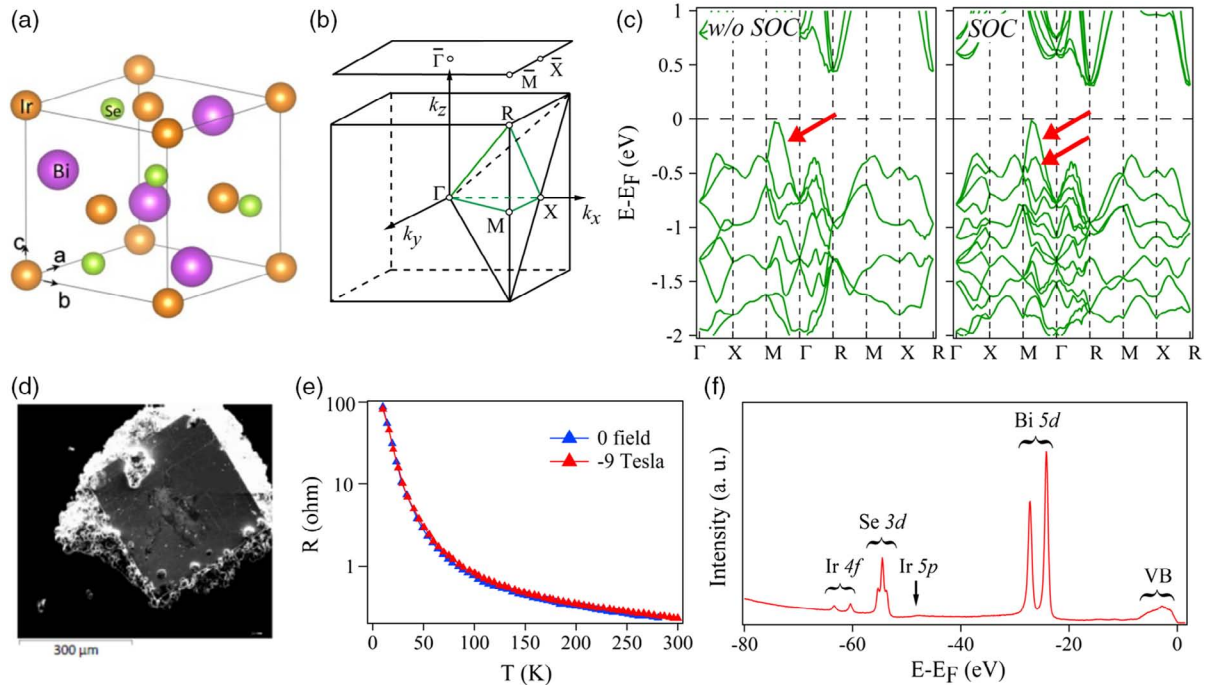


Figure 1. a) Crystal structure of IrBiSe. b) The BZ and high-symmetry points of the simple cubic structure. The $\bar{\Gamma}-\bar{M}-\bar{X}$ plane is the projected BZ perpendicular to k_z . Note that the actual irreducible part is larger than the volume enclosed by the green lines due to the absence of a center of inversion. c) Band structure from first-principle calculations without and with SOC. The red arrows indicate SOC induced a giant (≈ 0.3 eV) Dresselhaus splitting bulk band near E_F . d) Single crystal of IrBiSe. e) Temperature-dependent electrical resistance. f) Integrated photoemission spectrum using 110 eV horizontal polarized light.

not a half-Heusler compound).^[37,38] Its unit cell and corresponding Brillouin zone (BZ) are shown in **Figure 1a,b**, respectively. Note, that $\Gamma-M$ is not a symmetry line. Only $\Gamma-X$ (C2) and $\Gamma-R$ (C3) are. The crystal structure can also be thought of as a network of distorted IrBi_3Se_3 octahedra with each Bi or Se ion belonging to three such octahedra (Figure S1, Supporting Information). The samples used for the experimental studies were characterized by transport (Figure 1e) and integrated photoemission measurements (Figure 1f). The characteristic peaks in the latter spectrum suggest high-quality samples. The electrical resistance of IrBiSe as a function of temperature is shown in Figure 1e. The resistance increases rapidly upon cooling the sample, which is well consistent with weak density of states (DOS) near E_F . Furthermore, Figure 1e demonstrates that IrBiSe is a nonmagnetic material^[38] as the electrical resistance shows no variation between zero field cooling and field cooling.

Results of the first-principle band structure calculations of IrBiSe with and without the inclusion of spin-orbit coupling (SOC) in the computational scheme are shown in Figure 1c. From these calculations we find that the top of the valence band is formed by strongly hybridized Bi p–Se p states whereas the bottom of the conduction band is dominated by Ir d e_g states hybridized with the former (Figure S2, Supporting Information). Because of being strongly influenced by the SOC, the bands in the vicinity of E_F are spin-split everywhere in momentum space, except at the high-symmetry points. Interestingly, the splitting is more significant for the valence band than it is for the conduction band. We also mention the presence of two rather rare dispersion

crossings at Γ point at -0.75 and -1.3 eV below E_F when SOC is not included. Unlike evenly degenerate Dirac crossings, two of the bands have linear dispersions whereas the middle one is quadratic with no linear term at Γ . They become split by SOC into two Dirac points (-1.1 and -1.6 eV) and two pairs of Weyl points (-0.8 and -1.4 eV) (see also Figure 3e for spin characters). The most remarkable feature of the electronic structure of IrBiSe is the top of the valence band formed by the strongly dispersive state along the $\Gamma-M$ direction. As follows from the comparison of the computational results, these are nondegenerate states, well split from the other bands below the gap. There are 12 such maxima in the cubic BZ, shown in Figure 1b, as dominated by symmetry.

The angle-resolved photoemission spectroscopy (ARPES) data are compared with corresponding bulk states of the calculations in **Figure 2**. We compare the momentum distribution of the spectral weight within a narrow energy window near E_F with the calculated result integrated over k_z in Figure 2a,b. As expected from the band structure shown in Figure 1c, projection on the (001) surface should give four in-plane features along the diagonals of the square BZ and another four features corresponding to the other eight out-of-plane maxima (each pair of them will have the same projection). The experimental map reveals these multiple spot-like features, i.e., bands are mostly found at the rim of the BZ. In principle, there are ineluctable discrepancies between experimental and calculation maps, because of matrix element effects and large-region Fermi surface (FS) measurement with a single-energy photon. At a given photon energy, momentum distribution map corresponds to

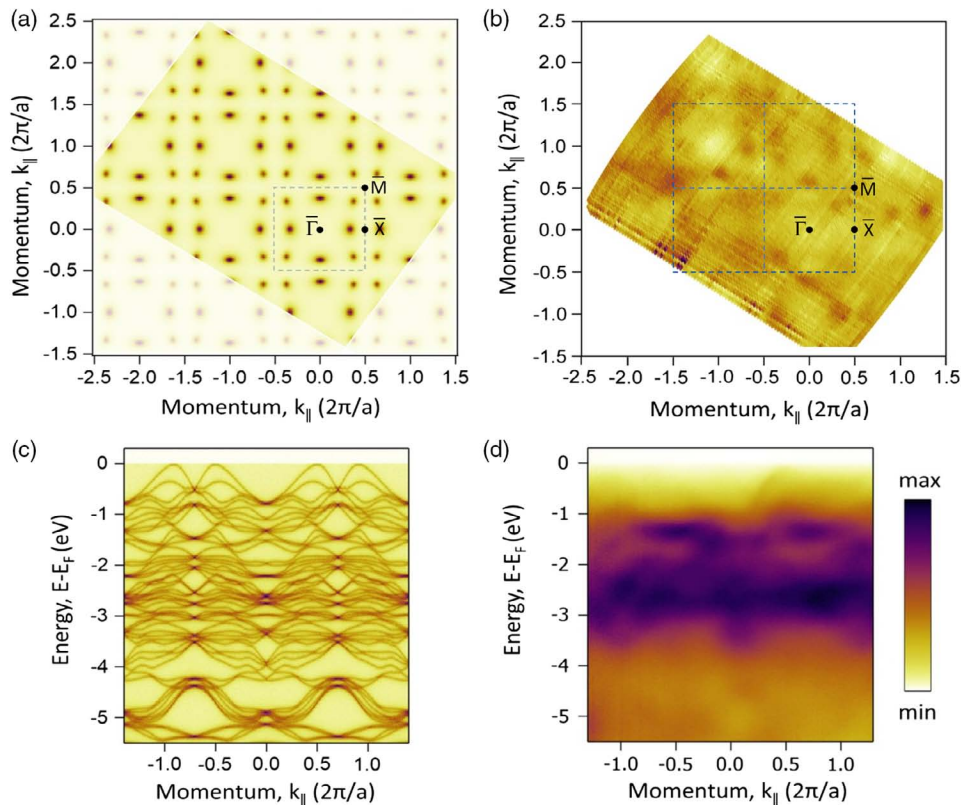


Figure 2. a) Calculated spectral weight just below E_F and integrated over k_z . b) Remnant FS map obtained by integrating over an energy window of 50 meV centered at E_F using 85 eV horizontal polarized light. c) Calculated spectral weight along the diagonal Γ – \bar{M} direction at $k_z = 0$. d) Photoemission intensity plot along the Γ – \bar{M} direction in (b).

constantly decreasing k_z values upon increasing absolute k_{\parallel} . In the first BZ, centered at (0, 0) in Figure 2b, four features on the diagonals mean that k_z here corresponds mostly to Γ plane, whereas in other repeated BZ the spots lying on verticals and horizontals are more pronounced.

We do not expect a full quantitative correspondence between the datasets shown in Figure 2c,d. Clearly catching only one of the low-energy features, the experimental data are broadened by temperatures, k_z limitation, and matrix element effects. Taking into account that low DOS near E_F induces weak photoemission signals, the overall agreement is still good and it is clear that the origin of the spots on the momentum distribution map is exactly the most intriguing feature of IrBiSe—namely, the presence of parabolic dispersion that is clearly splitting from the rest of the bands. Figure 2 further suggests that the detected band features near E_F are of mainly bulk origin.

Figure 3a,b shows the momentum–energy intensity distribution taken at different photon energies along the Γ – \bar{M} direction through the pair of closest spots on the map from Figure 2b and zoomed in toward E_F . Both plots show two maxima near E_F at different k values, though overlap bands exist at higher binding energy because of the matrix element effects and the k_z limitation in ARPES measurements. The k_{\parallel} splitting of the two maxima in Figure 3a,b is larger at 80 eV than at 75 eV evidencing the 3D character of these bands and suggesting that the former is closer to the Γ point along k_z direction. The corresponding

calculated data (right panels of Figure 3a,b) catch the main features, i.e., valence band maxima quite close to E_F and band splitting. From the second-derivative maps shown in middle panels of Figure 3a,b, we estimate a spin splitting of ≈ 270 meV, which is lower than the predicted value of 360 meV from the calculations. The experimental momentum offset of $\approx 0.4 \text{ \AA}^{-1}$ is consistent with the theoretical value of 0.43 \AA^{-1} .

The spin character of the two closest features was also estimated. However, the generally big noises in our many times spin-polarization ARPES measurements always blocked spin signals. We had to study the spin character with the help of circular dichroism (CD) by using circularly polarized light in Figure 3c. We are aware that CD cannot be directly related to the spin polarization because of matrix elements, but the observed strong dichroism can be considered as evidence for the very different spin characters of these features.

Figure 3d shows the spin splitting (ΔE) as a function of momentum (k) along different high-symmetry directions from the upper valence bands. In the figure, the curves with markers are the data, whereas the solid black lines are fits to the data using the equation $\Delta E = \alpha k + \gamma k^3$. The fits are good up to a momentum vector of 0.23 \AA^{-1} (47% of Γ – X width) from the zone center as shown in Figure 3d. From these fits we find that the spin splitting is linearly dependent on k for the bands in the Γ – X direction, whereas it is cubically dependent on k for the bands dispersing in the rest of the high-symmetry directions (Γ – M and X – R).

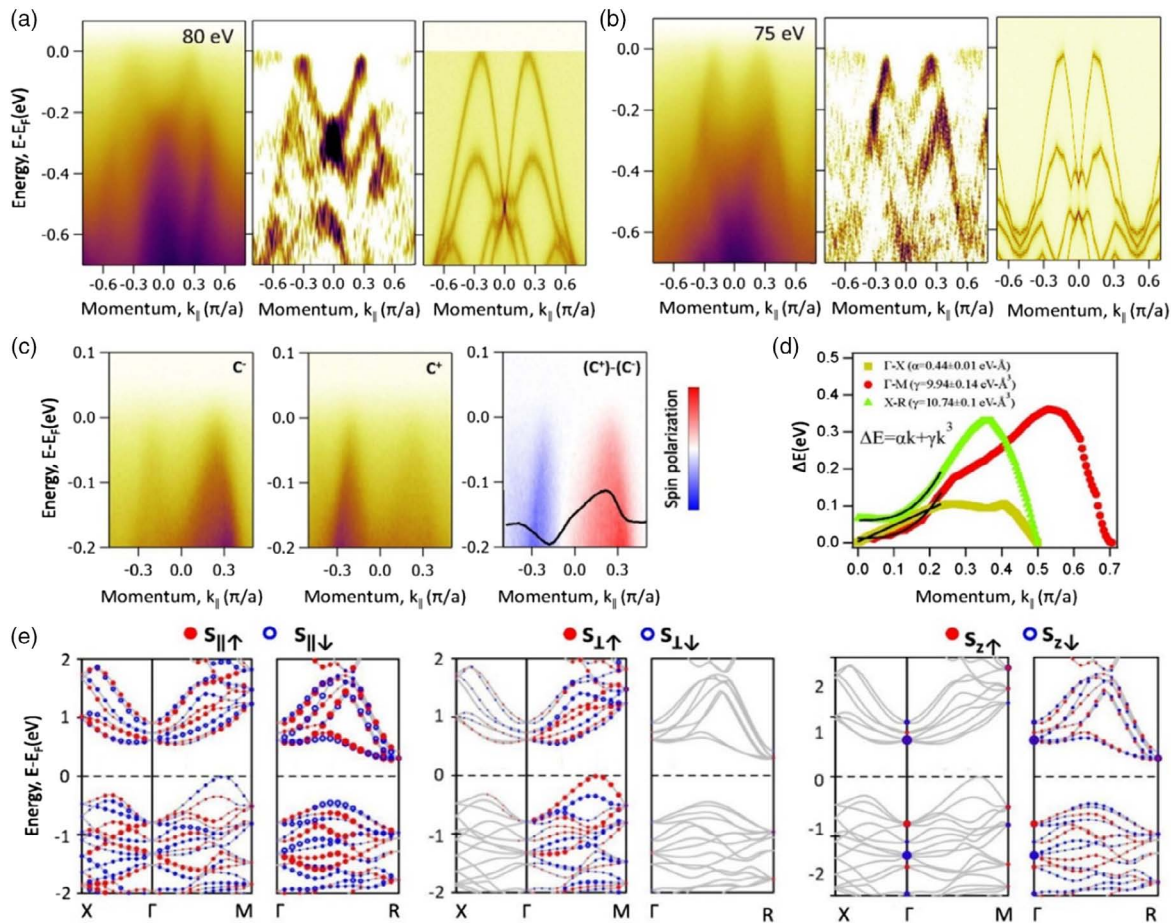


Figure 3. a,b) ARPES intensity and corresponding second-derivative plots along the $\bar{\Gamma}-\bar{M}$ direction in Figure 2b, but along the cuts going through the closest spots of the remnant FS, measured using 80 and 75 eV horizontal polarized light, respectively. Right panels are the corresponding calculated dispersions. c) Spectra recorded along the cuts going through the closest spots of the remnant FS with light of negative and positive helicities and their difference, i.e., the CD. d) Spin splitting (ΔE) as function of momentum (k) in different high-symmetry directions starting from the zone center. The black solid curves are the fits to the data using the equation shown in the figure. e) Spin polarization of the bands in IrBiSe. s_{\parallel} is a spin projection along the k direction. s_{\parallel} and s_z are spin projections perpendicular to the k direction. The symbol sizes are proportional to the spin polarization. One can see that the spins are parallel to k along ($\Gamma-X$), nearly orthogonal to k along ($\Gamma-M$), and nearly parallel to k along ($\Gamma-R$).

Furthermore, in the $\Gamma-X$ direction we estimate splitting parameters $\alpha = 0.44 \pm 0.01 \text{ eV \AA}$ and $\gamma = 0$, in the $\Gamma-M$ direction they are $\alpha = 0$ and $\gamma = 9.94 \pm 0.14 \text{ eV \AA}^3$, and in the $X-R$ direction they are $\alpha = 0$ and $\gamma = 10.74 \pm 0.1 \text{ eV \AA}^3$.

Finally, we present the theoretically defined spin characters of the bulk states of IrBiSe in Figure 3e. Spin projections onto the directions parallel and perpendicular to the given high-symmetry direction and to the k_z -axis are given by the size of the marker. Judging from the uneven distribution of the markers and their sizes on the plots, one can easily conclude that the electronic states near E_F display a peculiar spin texture. The occupied states along $\Gamma-X$ have spins oriented parallel to this direction, as middle and right panels containing $\Gamma-X$ show virtually no markers. The spin polarization of the discussed earlier highest occupied states is also well defined. These spins are directed almost perpendicular to $\Gamma-M$, having no k_z component, thus strongly reminiscent of the spin-momentum locking on the surfaces of the topological insulators.^[17]

We thus demonstrate that IrBiSe has a very peculiar electronic structure: there is only one—non-spin-degenerate and well split from others—dispersive electronic feature that approaches E_F , with spins directed nearly perpendicular to the momentum vector. This dispersion gives rise to the intriguing remnant FS consisting of spots at discrete values of momentum. In analogy to topological insulators, in most of which the chemical potentials do not cross bulk energy gaps at all and the realization of bulk insulating states needs doping, we will refer to IrBiSe as a “nonmagnetic half-metal” since its metallicity is a matter of light hole doping, which appears to be possible, and its FS is supported by electronic states having only one spin orientation. Unlike in ferro- or antiferromagnetic half-metals,^[7–13] the projection of the spin to the local axis rather than to a global axis is meant here. Obviously, such a unique and simple arrangement of valence electrons should imply the presence of interesting physics and a range of useful applications. Indeed, photoelectrons coming out of the sample upon hypothetical increase of photon energy of the exciting radiation from zero

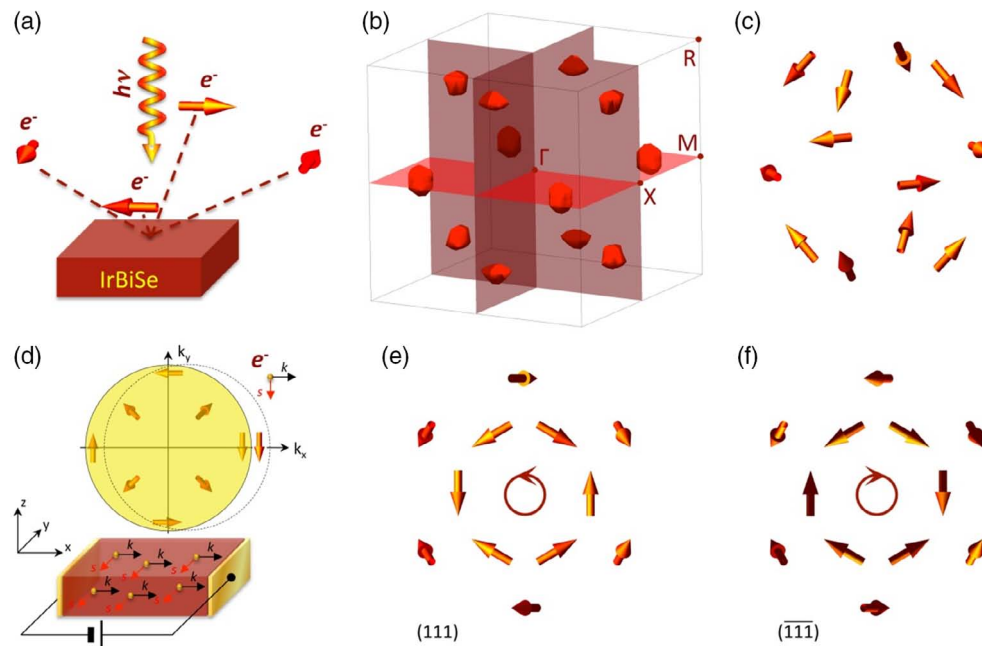


Figure 4. a) Schematic illustration of the emission of the spin-polarized electrons stimulated by photons. Here and in panel (d) sides of the crystal are along Γ - M . b) FS of lightly doped IrBiSe obtained by cutting the electronic structure of pristine compound 50 meV below E_F . c) Spins corresponding to the pockets of FS from (b). Here and in the following panels, spins are considered as perpendicular to momentum vectors. d) Schematics of generation of the spin-polarized current. e, f) Views on the spin texture from (111) and $(\bar{1}\bar{1}\bar{1})$ directions, respectively.

will be spin-polarized and to flip the spin polarization, one would just need to tilt or rotate the sample (instead of changing the light helicity, as in the GaAs case^[36,39]), switching from spot to spot of the remnant FS.

The FS of lightly hole-doped IrBiSe is shown in **Figure 4b**. Though the Fermi pockets are identical, their shape is not symmetric with respect to Γ - M , which is dominated by the symmetry of the irreducible part of the BZ (Figure 1b, Figure S3 and S4, Supporting Information). If projected to any of the coordinate planes, they will correspond to the spots on the remnant FS map shown earlier in Figure 2a,b. Each pocket is singly degenerate, meaning that only a band with one spin character crosses E_F . We have checked that all electronic states forming such small pockets have the same direction of spins in the local coordinate system (Figure S4, Supporting Information): they are all almost perpendicular to the momentum. Such an arrangement of spins results in a unique 3D spin texture shown in Figure 4c. An immediate association with the spin texture of the surface states in topological insulators springs to mind,^[14,17] but the case discussed here for IrBiSe is a 3D generalization of the bulk states. The spins are not tangential to the circle, but nearly tangential to the 12 points on the sphere in momentum space. Such a spin texture of the states at the E_F guarantees the absence of backward scattering events in any of these directions as the spins for opposite momenta are always opposite to each other. This is a very desirable property for a spintronics-relevant material where long coherence times of spin-polarized electrons are essential, as is a 3D single crystal material with a simple cubic crystal structure.

Recent experimental studies have reported electrical detection of earlier-predicted current-induced spin polarization on the surfaces of topological insulators.^[40] We anticipate a similar

effect in lightly hole-doped IrBiSe, but that the spin-polarized currents will be generated in the bulk, rather than on the fragile surface. Indeed, application of an electric field along any of the 12 directions corresponding to Γ - M (Figure 4d) will produce a net momentum along the k_x direction. This is indicated by the shifted projection to the (k_x, k_y) plane of the sphere mentioned earlier; the top view is shown in the upper part of Figure 4d. This shift will result in an electric current along x , which also induces a spin current with spins oriented along $-y$. The only difference with the case of topological insulators is that there are two more crossings of E_F along the Γ - M direction with Fermi velocities of the opposite sign. Their presence could reduce the spin polarization of the current, but the significant inequality in the absolute values of the Fermi velocities of the electrons, moving along x with spins oriented along $-y$ and y , will guarantee the effect. Thus, by putting a usual current through such a sample one can generate a flow of spin-polarized electrons and its amplitude and direction can be controlled by the initial current. Considering the 3D spin texture along the (111) direction, one notices its chirality, dominated by the C_3 symmetry and absence of center of inversion in IrBiSe. Negative and positive helicities are shown in Figure 4e,f, respectively. This chirality should give a different response when interacting with circularly polarized light and could possibly be used as a spin sensor, e.g., in spin-polarized scanning tunneling microscope tips.

In addition, it is very intriguing to ask whether doped IrBiSe will become superconducting at low temperatures. On one hand, when the pockets are very small, there are ideal conditions for electrons to pair up as all of them will have a counterpart with opposite k and s . On the other hand, when the doping is sufficiently large, so that the electrons can pair up within a given pocket,

the superconductivity will be of the triplet type as all electrons corresponding to this pocket will have the same spin. Moreover, the material could possibly host also the Fulde–Ferro–Larkin–Ovchinnikov (FFLO) phase with finite momentum of the condensate since the FSs for opposite spin directions are already different and presence of the strong magnetic field is not necessary. Our findings indicate that IrBiSe could play a significant role in further solving both fundamental puzzles of physics and practical problems of realization of highly efficient spintronic devices.

Supporting Information

Supporting Information is available from the Wiley Online Library or from the author.

Acknowledgements

The authors are grateful to Martin Knupfer for the fruitful discussion. This work was supported under DFG grant 1912/7-1. Z.L. acknowledges support by the National Natural Science Foundation of China (11704394). S.T. acknowledges support by the Department of Science and Technology, India, through the INSPIRE-Faculty program (IFA14 PH-86). The work at Princeton University was supported by NSF MRSEC grant DMR 1420541 and the ARO MURI on topological insulators, grant W911NF-12-1-0461.

Conflict of Interest

The authors declare no conflict of interest.

Keywords

angle-resolved photoemission spectroscopy, band structure, IrBiSe, first-principles calculations, spin texture

Received: December 5, 2019

Revised: February 4, 2020

Published online: February 12, 2020

- [1] R. A. de Groot, F. M. Müller, P. G. Engen, K. H. J. Buschow, *Phys. Rev. Lett.* **1983**, *50*, 2024.
- [2] J. Park, E. Vescovo, H. J. Kim, C. Kwon, R. Ramesh, T. Venkatesan, *Nature* **1998**, *392*, 794.
- [3] H. Leuken, R. A. Groot, *Phys. Rev. Lett.* **1995**, *74*, 1171.
- [4] I. Žutić, J. Fabian, S. Sarma, *Rev. Mod. Phys.* **2004**, *76*, 323.
- [5] X. Hu, *Adv. Mater.* **2011**, *24*, 294.
- [6] V. K. Joshi, *Eng. Sci. Technol. Int. J.* **2016**, *19*, 1503.
- [7] G. M. Müller, J. Walowski, M. Djordjevic, G. X. Miao, A. Gupta, A. V. Ramos, K. Gehrke, V. Moshnyaga, K. Samwer, J. Schmalhorst, A. Thomas, A. Hütten, G. Reiss, J. S. Moodera, M. Münzenberg, *Nat. Mater.* **2008**, *8*, 56.
- [8] X. Wan, M. Kohn, X. Hu, *Phys. Rev. Lett.* **2005**, *94*, 087205.
- [9] W. E. Pickett, *Phys. Rev. B* **1998**, *57*, 10613.
- [10] Y. Nie, X. Hu, *Phys. Rev. Lett.* **2008**, *100*, 117203.
- [11] K. Kobayashi, T. Kimura, H. Sawada, K. Terakura, Y. Tokura, *Nature* **1998**, *395*, 677.
- [12] Y.-W. Son, M. L. Cohen, S. G. Louie, *Nature* **2006**, *444*, 347.
- [13] K. Ueda, H. Tabata, T. Kawai, *Science* **1998**, *280*, 1064.
- [14] M. Z. Hasan, C. L. Kane, *Rev. Mod. Phys.* **2010**, *82*, 3045.
- [15] Z. Wang, H. Weng, Q. Wu, X. Dai, Z. Fang, *Phys. Rev. B* **2013**, *88*, 125427.
- [16] X. Wan, A. M. Turner, A. Vishwanath, S. Y. Savrasov, *Phys. Rev. B* **2011**, *83*, 205101.
- [17] P. Roushan, J. Seo, C. V. Parker, Y. S. Hor, D. Hsieh, D. Qian, A. Richardella, M. Z. Hasan, R. J. Cava, A. Yazdani, *Nature* **2009**, *460*, 1106.
- [18] E. Haubold, K. Koepf, D. Efremov, S. Khim, A. Fedorov, Y. Kushnirenko, J. Brink, S. Wurmehl, B. Büchner, T. K. Kim, M. Hoesch, K. Sumida, K. Taguchi, T. Yoshikawa, A. Kimura, T. Okuda, S. V. Borisenko, *Phys. Rev. B* **2017**, *95*, 241108.
- [19] M. Aitani, Y. Sakamoto, T. Hirahara, M. Yamada, H. Miyazaki, M. Matsunami, S. Kimura, S. Hasegawa, *Jpn. J. Appl. Phys.* **2013**, *52*, 110112.
- [20] C. I. Fornari, P. H. O. Rappl, S. L. Morelão, T. R. F. Peixoto, H. Bentmann, F. Reinert, E. Abramof, *APL Mater.* **2016**, *4*, 106107.
- [21] S. Datta, B. Das, *Appl. Phys. Lett.* **1990**, *56*, 665.
- [22] I. Gierz, T. Suzuki, E. Frantzeskakis, S. Pons, S. Ostanin, A. Ernst, J. Henk, M. Grioni, K. Kern, C. R. Ast, *Phys. Rev. Lett.* **2009**, *103*, 046803.
- [23] J. M. Riley, F. Mazzola, M. Dendzik, M. Michiardi, T. Takayama, L. Bawden, C. Granerød, M. Leandersson, T. Balasubramanian, M. Hoesch, T. K. Kim, W. Meevasana, P. Hofmann, M. S. Bahramy, J. W. Wells, P. D. C. King, *Nat. Phys.* **2014**, *10*, 1745.
- [24] J. Nitta, T. Akazaki, H. Takayanagi, T. Enoki, *Phys. Rev. Lett.* **1997**, *78*, 1335.
- [25] D. D. Sante, P. Barone, R. Bertacco, S. Picozzi, *Adv. Mater.* **2013**, *25*, 509.
- [26] M. Liebmann, C. Rinaldi, D. Sante, J. Kellner, C. Pauly, R. N. Wang, J. E. Boschker, A. Giussani, S. Bertoli, M. Cantoni, L. Baldrati, M. Asa, I. Vobornik, G. Panaccione, D. Marchenko, J. Sánchez-Barriga, O. Rader, R. Calarco, S. Picozzi, R. Bertacco, M. Morgenstern, *Adv. Mater.* **2016**, *28*, 560.
- [27] J. Krempaský, H. Volfová, S. Muff, N. Pilet, G. Landolt, M. Radović, M. Shi, D. Krieger, V. Holý, J. Braun, H. Ebert, F. Bisti, V. A. Rogalev, V. N. Strocov, G. Springholz, J. Minár, J. H. Dil, *Phys. Rev. B* **2016**, *94*, 205111.
- [28] S. LaShell, B. A. McDougall, E. Jensen, *Phys. Rev. Lett.* **1996**, *77*, 3419.
- [29] Y. M. Koroteev, G. Bihlmayer, J. E. Gayone, E. V. Chulkov, S. Blügel, P. M. Echenique, P. Hofmann, *Phys. Rev. Lett.* **2004**, *93*, 046403.
- [30] M. Hoesch, M. Muntwiler, V. N. Petrov, M. Hengsberger, L. Patthey, M. Shi, M. Falub, T. Greber, J. Osterwalder, *Phys. Rev. B* **2004**, *69*, 241401.
- [31] C. R. Ast, J. Henk, A. Ernst, L. Moreschini, M. C. Falub, D. Pacilé, P. Bruno, K. Kern, M. Grioni, *Phys. Rev. Lett.* **2007**, *98*, 186807.
- [32] S. V. Ereemeev, I. A. Nechaev, Y. M. Koroteev, P. M. Echenique, E. V. Chulkov, *Phys. Rev. Lett.* **2012**, *108*, 246802.
- [33] G. Landolt, S. V. Ereemeev, O. E. Tereshchenko, S. Muff, B. Slomski, K. A. Kokh, M. Kobayashi, T. Schmitt, V. N. Strocov, J. Osterwalder, E. V. Chulkov, J. H. Dil, *New J. Phys.* **2013**, *15*, 085022.
- [34] S. V. Ereemeev, I. P. Rusinov, I. A. Nechaev, E. V. Chulkov, *New J. Phys.* **2013**, *15*, 075015.
- [35] K. Ishizaka, M. S. Bahramy, H. Murakawa, M. Sakano, T. Shimojima, T. Sonobe, K. Koizumi, S. Shin, H. Miyahara, A. Kimura, K. Miyamoto, T. Okuda, H. Namatame, M. Taniguchi, R. Arita, N. Nagaosa, K. Kobayashi, Y. Murakami, R. Kumai, Y. Kaneko, Y. Onose, Y. Tokura, *Nat. Mater.* **2011**, *10*, 521.
- [36] G. Dresselhaus, *Phys. Rev.* **1955**, *100*, 580.
- [37] F. Hulliger, *Nature* **1963**, *198*, 382.
- [38] F. Hulliger, E. Mooser, *J. Phys. Chem. Solids* **1965**, *26*, 429.
- [39] J. W. Luo, G. Bester, A. Zunger, *Phys. Rev. Lett.* **2009**, *102*, 056405.
- [40] C. H. Li, O. M. J. Erve, J. T. Robinson, Y. Liu, L. Li, B. T. Jonker, *Nat. Nanotechnol.* **2014**, *9*, 218.